Published in final edited form as:
Dev Dyn. 2009 May ; 238(5): 1033–1041. doi:10.1002/dvdy.21925.

Three-dimensional visualisation of testis cord morphogenesis, a novel tubulogenic mechanism in development

Alexander N. Combes[1], **Emmanuelle Lesieur**[1], **Vincent R. Harley**[2], **Andrew H. Sinclair**[3], **Melissa H. Little**[1], **Dagmar Wilhelm**[1], and **Peter Koopman**[1,4]

[1]Division of Molecular Genetics and Development, Institute for Molecular Bioscience, The University of Queensland, Brisbane, QLD 4072, Australia

[2]Prince Henry's Institute of Medical Research, Melbourne, VIC 3168, Australia

[3]Murdoch Children's Research Institute, and Department of Paediatrics, University of Melbourne, Royal Children's Hospital, Melbourne, VIC 3052, Australia

Abstract

Testis cords are specialised tubes essential for generation and export of sperm, yet the mechanisms directing their formation, and the regulation of their position, size, shape and number, remain unclear. Here, we use a novel fluorescence-based three-dimensional modelling approach to show that cords initially form as a network of irregular cell clusters that are subsequently remodelled to form regular parallel loops, joined by a flattened plexus at the mesonephric side. Variation in cord number and structure demonstrates that cord specification is not stereotypic, although cord alignment and diameter becomes relatively consistent, implicating compensatory growth mechanisms. Branched, fused and internalised cords were commonly observed. We conclude that the tubule-like structure of testis cords arise through a novel form of morphogenesis consisting of coalescence, partitioning, and remodelling. The methods we describe are applicable to investigating defects in testis cord development in mouse models, and more broadly, studying morphogenesis of other tissues.

Introduction

Testis cords are specialised tubular structures that facilitate male reproduction by sheltering germ cells from exogenous signals, nurturing their development into mature spermatogonia, and canalising them into the male reproductive tract. Testis cord development is a hallmark of success for the male sex determining pathway, which must overcome competing signals to wrest the gonad from an ovarian fate (Kim et al., 2006). An increasing understanding of cellular events during testis development is building the potential for this organ as a model of tissue organisation, with the process of cord formation being of central interest.

During early differentiation of the testis, pre-Sertoli and germ cells form apparently random clusters. Further elaboration of these clusters into definitive cords does not rely on the presence of germ cells (Buehr et al., 1993b), but instead on cell migration from the mesonephros (Buehr et al., 1993a; Merchant-Larios et al., 1993; Martineau et al., 1997; Tilmann and Capel, 1999; Combes et al., 2008). Testis cords are encased by smooth muscle-like peritubular myoid cells, but recent studies have revealed that peritubular myoid cells do not come from the mesonephros or trigger cord formation (Combes et al., 2008; Cool et al., 2008). Instead, migrating endothelial cells induce Sertoli cells to arrange into cords (Buehr

[4]Author for correspondence: Tel: +61 7 3346 2059, Fax: +61 7 3346 2101, p.koopman@imb.uq.edu.au.

et al., 1993a; Merchant-Larios et al., 1993; Martineau et al., 1997; Tilmann and Capel, 1999; Combes et al., 2008), and interaction between Sertoli and peritubular myoid cells leads to production, and polarised secretion, of various extracellular matrix proteins between these two cell types (Paranko et al., 1983; Pelliniemi et al., 1984; Paranko, 1987; Frojdman et al., 1989; Frojdman et al., 1992). Thus, details are emerging of how various cell types contribute to testis cord formation.

In the mouse gonad, testis cords develop from 11.5 days *post coitum* (dpc) and are visible by 12.5 dpc under a dissecting microscope. However, using conventional light microscopy, the structure of cords is obscured by tissue opacity. Analysis of tissue sections circumvents this problem but sacrifices the three-dimensional context of cords. Thus, there is a need for a method that enables analysis of cord structure at high resolution throughout the entire gonad. Some progress has been made towards this goal through reconstruction of serial sections from a portion of fetal rabbit gonads (Wartenberg et al., 1991) and through serial optical sections of a genital ridge obtained by confocal microscopy (Karl and Capel, 1995). Recent work in mouse has used fluorescence and differential contrast imaging to explore the close spatial relationship between ingressing vasculature and developing cords (Coveney et al., 2008). Despite these advances, important questions remain regarding cord structure, size, shape, position and number, and the mechanisms regulating these features.

To address these questions, we developed a new method for visualising organ development in three dimensions. Application of this method revealed that the structure of testis cords arises through remodelling of a primitive cord network in an entirely novel mode of tubulogenesis. Our data implicate mechanisms that generate cords of similar size from irregular initial clusters, and molecular differences between the mesonephric face of the gonad and the rest of the gonad that result in different cord properties in these two domains. The methods we describe are applicable to investigating defects in testis cord development in mouse models, and to studying the morphogenesis of other organs.

Results

As a first step in examining the specification, structure, and number of testis cords in mice, we used *in situ* hybridisation (ISH) on whole testes between 12.5 and 15.5 dpc to visualise testis cords using the germ cell marker *Oct-4* (Scholer et al., 1990).

At 12.5 dpc, primitive testis cords were observed throughout the gonad (Fig. 1A). A ring of staining was observed in transverse slices of the central region of the testis, confirming the basic toroid (cylindrical ring) structure of testis cords at this stage (Fig. 1B). By 13.5 dpc, cord numbers appeared to have decreased, and definitive cords occupied the entire gonad (Fig. 1C). Variation in cord structure was identified with apparent instances of cord branching or overlap (Fig. 1C,E,G, white arrowheads). Transverse slices demonstrated a change in the profile of cords as the testis matures. The toroid structure observed in central cords at 12.5 dpc developed into an inverted ‘U’ shape from 14.5 dpc (Fig. 1B,D,F,H, black arrowheads) suggesting remodelling of cord structure, or movement of germ cells away from the mesonephric area. At 15.5 dpc, some cords buckled under the surface of the gonad, potentially due to physical constraints (Fig. 1H, red arrowhead). These results reveal two novel features of the cord network. First, cord numbers appear to decrease between 12.5 and 13.5 dpc. Second, some cords deviate from a simple loop structure through branch points. These phenomena have received little attention in previous studies, prompting their further investigation here.

3-D modelling of cord structure

To clarify in detail how cords are structured and remodelled, we required a visualisation method that would enable high-resolution analysis of cord structure throughout the entire gonad. Through assessing different testis cord markers by confocal microscopy, we found that a fluorescently labelled anti-mouse secondary antibody, goat anti-mouse Alexa 555 (555), produced an avid histological stain. Using this antibody we achieved a uniform signal throughout the depth of the whole-mount tissue, defining cords in a much clearer way than any cell type-specific marker tested. In whole mount or tissue sections, 555 bound and labelled all cells in the tissue with a higher affinity for mesenchymal cells and basement membranes. In the testis, the basement membrane surrounding the testis cords was strongly labelled from 12.5 dpc, providing high definition of cord structure (Fig. 2A,B). The vasculature and interstitium were also stained, but did not obscure the outline of the cords (Fig. 2A,B). The structures defined by 555 were confirmed by comparison to basement membrane marker laminin (data not shown), Sertoli cell marker SOX9 (Fig. 2A,C), and vascular marker VE-cadherin (Fig. 2A,D).

To analyse cord structure, we collected high resolution optical sections of whole mount testes stained with 555. We then outlined cord boundaries and reconstructed 3-D models for multiple samples from 12.5–15.5 dpc (Fig. 3). 3-D animations of one model for each time point have been appended as supporting data (Supplementary movies 1–4). Lateral views of the models (Fig. 3B,F,J,N) replicate lateral views of cords seen in wholemount ISH (Fig. 1), further confirming the accuracy of this method. The resolution of our models enabled visualisation of the network of testis cords to an unprecedented level of detail, allowing us to characterise several features of testis cord morphogenesis.

Variation in cord number and structure

One important clue to understanding the mechanisms driving testis morphogenesis is to determine to what degree cord formation is a stereotypic process, and which elements within the system vary. All developing testes have the basic form of a series of looped cords arranged in parallel across the length of the gonad. One analysis of cord formation put the number of cords at ~10 (Coveney et al., 2008), yet it remains unclear whether the structure or number of cords varies between gonads of the same species and age.

Nascent cords in 12.5 dpc testes varied greatly in shape and size, and appeared to be transitional structures between clusters and definitive cords. Testes mature earliest in the centre and later in the poles (Bullejos and Koopman, 2001), and this spatial gradation is reflected in the state of development of the testis cords visualized in this study. Regions near the poles of the testis were generally more perforated, interconnected and irregular, such that it was difficult to distinguish one cord from another (Fig. 3B, C, arrowheads). Cords in the central area of the gonad were more distinct, but still irregular in form and diameter (Fig. 3B, C). The co-existence of these stages in the same testis implies that developing testis cords are rapidly and dynamically remodelled, and the progression of 12.5 dpc protocords into definitive cords by 13.5 dpc may involve fusion of smaller cords and irregularities into larger, more stable structures. The remodelling of cord structure is so thorough that it is not possible to predict the structure, position or likely number of definitive cords at 13.5 dpc by their form at 12.5 dpc.

Cord structure also varied considerably in more mature testes. Most cords formed a toroidal loop under the coelomic epithelium, originating and terminating at the mesonephric border (Fig. 3). Some were connected with adjacent cords at other positions and either fused (Fig. 4A, blue), or split into two at lateral branch points (Fig. 4A, red). Transverse views of the models revealed the presence of internal cords that either branched internally from an

external cord (Fig. 4B,C, orange), or existed as whole looped cords that occupy the internal space (Fig. 4C, yellow; Supplementary movie 5). The variation in structure between individual cords indicates the influence of a stochastic or exogenous factor during cord establishment.

Internal testis cords

Internal cords are usually hidden from view by external cords that abut the coelomic epithelium, and therefore have been largely overlooked. Using the 3-D models to interrogate the entire network of testis cords, we counted the number of cords from at least three models for each time point from 12.5 to 14.5 dpc (Fig. 4D). We initially analysed numbers of external (those seen on the surface of a model) and internal (all others) cords separately. We found a reduction in the number of external testis cords from 12±1.5 at 12.5 dpc, to 9±1 at 13.5 and 14.5 dpc ($p<0.05$; Fig. 4D). However, the number of internal cords increased from 0.3±0.5 at 12.5 dpc, to 5.2±1.6, then 7±1.2 at 13.5 and 14.5 dpc respectively ($p<0.005$ for the increase between 12.5 and 14.5). Thus, the reduction in external cords seen between 12.5 and 13.5 dpc is offset by an increase in internal cord numbers, resulting in a similar total number of testis cords between 12.5–14.5 dpc (12.5 dpc = 13.6±2.3; 13.5 dpc = 14±1.6; 14.5 = 16.8±1.7; Fig. 4E).

We reasoned that the redistribution of some cords from external to internal positions from 12.5 to 13.5 dpc (Fig. 4D) might be driven by spatial constraints. To investigate this hypothesis we determined and compared the average cord diameter and gonad length for 12.5 and 13.5 dpc gonads. The average diameter of cords in the coelomic region doubled between 12.5 and 13.5 dpc (42±2 μm [n=63] to 84±3 μm [n=60]; $p<0.0005$), whereas the length of the gonad increased by only 10% (1027±84 μm [n=6] to 1150±45 μm [n=9]; $p>0.05$), suggesting that some cords are literally squeezed into internal positions as the testis matures, presumably due to physical pressure.

Development of the rete primordium

One feature of testis development that has remained obscure is the region towards the mesonephric face of the testis, where the cords are assumed to connect with each other. Our analysis shows that this region does not become segmented, but remains as a broad, flattened plexus (network) with perforations (Fig. 3D) that presumably correlate to paths of vascular ingression from the mesonephros (Combes et al., 2008; Coveney et al., 2008). In gonads at later time points, this plexus had contracted and narrowed to occupy the dorso-medial region of the gonad (Fig. 3H,L,P). Thus, we confirm that testis cords interconnect through a plexus at the mesonephric side of the gonad.

Anatomically, this plexus occupies a similar area to that in which the rete testis later forms. The rete testis is the connection between the testis cords and the mesonephric tubules. We investigated connections between the gonad and mesonephros and found that this plexus connects the network of cords to the mesonephric tubules by 15.5 dpc (Fig. 5; Supplementary movie 6). From this, we conclude that the plexus is the precursor of the rete testis, a collection point for sperm to be exported from the testis, and we subsequently refer to it as the rete primordium.

Cord remodelling in the mesonephric and coelomic regions of the testis

The flattened, perforated network of the rete primordium provides a stark contrast to the arrayed tubule-like structures of the testis cords in the coelomic region of the gonad and raises the questions of how and when these structural differences are established. To address these questions, we compared cord structure in coelomic and mesonephric regions from 12.25 to 13.5 dpc. Lateral views of testis cord models at 12.25 dpc showed little evidence of

cord partitioning compared to models from 12.5 and 13.5 dpc (Fig. 6A–C). However, internal views of the same samples showed extensive segregation of the gonad into irregular cord domains (Fig. 6D). By 13.5 dpc, the irregular domains had resolved into cords in the coelomic region, and into a flattened plexus in the mesonephric region (Fig. 6E,F). At 12.25 dpc, cord diameter was similar in coelomic and mesonephric regions (Fig. 6G). By 13.5 dpc the mean cord diameter between coelomic and mesonephric regions had diverged: cord diameter in the coelomic region had roughly doubled (54 to 84 μm), but in the mesonephric region had halved (47 to 22 μm; Fig. 6G). Cord diameter was consistent within each region. These data demonstrate that testis cords in the coelomic and mesonephric regions of the gonad actively remodel into one of two different forms, despite a common beginning.

Discussion

In this study we developed and exploited novel fluorescence-based imaging methods to build a picture of how tests cords develop in three dimensions. It is well established that testis cords are looped, parallel tubes arranged transverse to the long axis of the testis, and that these tubes link up at the mesonephric face of the testis. However, our studies reveal several issues that have remained unclear from previous methods of imaging, and highlight a number of new aspects about the dynamics of testis cord formation. We show, for example, that the number of cords (approx. 14) is higher than previously suspected, because several cords in each gonad are internal and therefore not obvious by standard imaging techniques. Cords arise from apparently randomly partitioned clusters of pre-Sertoli cells and germ cells, indicating a stochastic initial patterning process. Irregularities in cord structure, such as fused or branched cords, are a common feature, and testis cord numbers are variable, reflecting these stochastic beginnings. Immature cords arising from these clusters are rapidly remodelled to result in definitive cords, and the remodelling occurs differently in the mesonephric and coelomic domains of the testis, giving rise to the rete primordium and the definitive cords, respectively. The remodelling in the coelomic domain achieves the regularity in form and orientation seen in definitive testis cords. These findings indicate that cord formation is not a stereotypical process, and bring into focus the underlying mechanisms regulating this novel mode of tubulogenesis.

Existing models regarding how testis cords are formed invoke a partitioning or repulsive action for migrating endothelial cells as they traverse the gonad (Combes et al., 2008; Coveney et al., 2008). When endothelial cell-cell contacts were disrupted with a mild dose of blocking antibody to VE-cadherin, testis vasculature formed a hyperbranched network that was distributed throughout the gonad (Combes et al., 2008). This indicates that the spacing of vessels does not arise through pre-determination of migration paths, but is stochastically established, and maintained through endothelial cell-cell adhesion. Because endothelial cells direct cord partitioning, it follows that the initial partitioning of testis cords is also stochastic. Consistent with this concept, we see large variation in cord structure and size as cords are first defined, and in varying cord numbers and structure as the testis matures. However, relative uniformity in alignment and diameter of cords suggests the involvement of a homeostatic mechanism that contributes to a more regular definitive cord structure to compensate for the stochastic nature of their establishment.

Our model of cord formation through coalescence and partitioning (Combes et al., 2008) centres around migrating endothelial cells partitioning the testis cords as they traverse the gonad. Yet endothelial cells migrate through the testis in columnar streams (Coveney et al., 2008). Therefore, if the presence of endothelial cells causes localised cord partitioning, and is the only factor to influence cord structure, then we would expect the testis to develop into a perforated structure, like Swiss cheese, rather than the parallel cords, which resemble a stack of doughnuts. Our imaging data reveal that the form and position of cords is not

finalised during cord partitioning. Rather, the initial partitioning event results in a randomised cord network at ~12.25 dpc, with this network undergoing remodelling and/or refinement to form the rete primordium and the regular looped structure of cords as development progresses. This conclusion is supported by the findings of Wartenberg and colleagues (Wartenberg et al.), who reported remodelling of the cords from a primary reticulum in rabbit testes. Mature Sertoli cells have an innate capacity to form cords (Gassei and Schlatt, 2007) although in the context of the embryo, this capacity is not realised without interaction with migrating endothelial cells (Buehr et al., 1993a; Merchant-Larios et al., 1993; Martineau et al., 1997; Tilmann and Capel, 1999; Combes et al., 2008). Thus, it is not surprising that the initial random partitioning of clusters of Sertoli cells resolves into cords. However, the regular alignment of looped cords along the length of the gonad, and their anchoring at the mesonephric side, point to the influence of patterning mechanisms that remain to be identified.

We propose that cord branches arise as a result of this process of partitioning and remodelling. The variation involved in the initial partitioning event gives rise to varied cord structures—some form independent loops, while others remain interconnected with near-by cell clusters. During testis development these structures mature, with independent loops forming classic testis cords, and structures that had retained interconnections from their partitioning appearing as branched cords. This process is clearly distinct from branching morphogenesis that occurs in the lung and kidney, because cords do not appear to branch from a bud, but seem to spontaneously organise after partitioning.

Despite common beginnings, cord structures come to differ in coelomic and mesonephric regions of the gonad. In the coelomic region of the gonad, Sertoli cell clusters typically evolve into the looped cord structures that originate from and return to the mesonephric region. In contrast, similar clusters in the mesonephric region form a flattened, interconnected plexus which is the precursor of the rete testis. How might these differences arise? One possibility is that cord structure may be modulated by a regionally restricted morphogen. We examined testis-associated gene expression patterns in the GenitoUrinary Development Molecular Anatomy Project database (GUDMAP; Little et al., 2007; McMahon et al., 2008; www.gudmap.org/) and observed gene expression localised to the mesonephros, or along the border between the gonad and mesonephros (Supplementary Fig. 1 and Supplementary Table 1). Genes expressed in either of these domains may exert a localised effect on the Sertoli cells near that region by either suppressing the partitioning of cords, or promoting the development and refinement of the rete primordium into the rete testis. Members of the insulin-, and transforming growth factor-beta- signalling pathways were expressed within these domains, and are capable of regulating such morphogenesis. However, further studies are required to test if these genes, or others, regulate the regional differences in cord morphology across the testis.

Tubulogenesis is a recurring mode of morphogenesis during embryonic development, and is known to occur through several distinct mechanisms. Both kidney and lung undergo a process of branching morphogenesis whereby an existing tubular bud is induced to sprout and branch according to molecular cues received from the surrounding environment (Pohl et al., 2000). In contrast, a process of invagination and fusion generates the neural tube (Catala et al., 1996), while polarisation then cavitation of a cord of cells into a luminal tubule contributes to Müllerian duct formation and secondary neurulation (Catala et al., 1996; Orvis and Behringer, 2007). Clearly, testis cords do not arise through these established modes of tube formation but through a process of coalescence, partitioning, and remodelling —a previously uncharacterised and so far unique mode of tubulogenesis. Further study of this process is likely to uncover new insights into tubulogenic mechanisms used more broadly in organogenesis.

Experimental Procedures

Mouse strains

Embryos were collected from timed matings of outbred CD1 strain, with noon of the day on which the mating plug was observed designated 0.5 dpc.

Whole-mount *in situ* hybridization (ISH)

Embryos and dissected gonads/mesonephroi were fixed in 4% paraformaldehyde (PFA) in phosphate buffered saline (PBS) for several hours at 4°C. ISH with digoxygenin (DIG)-labeled RNA probe for *Oct-4* (Scholer et al., 1990) was carried out essentially as described by Hargrave at al. (2006).

Antibodies

Rabbit anti-SOX9 antibody has been described previously (Wilhelm et al., 2005). A rat antibody specific for vascular endothelial cadherin (VE-Cadherin) was obtained from BD Biosciences and used at a dilution of 1:200. All secondary antibodies, goat anti-rat Alexa Fluor 647, goat anti-rabbit Alexa Fluor 488, goat anti-rabbit Alexa Fluor 647, and goat anti-mouse Alexa Flour 555 were obtained from Invitrogen and used at a dilution of 1:200.

Whole mount immunofluorescence

Tissue samples were fixed in 4% PFA for 1–4 h or overnight before blocking for 4 h in PBS with 0.1% Triton x-100 (PBTX) and 10% heat inactivated horse serum (Invitrogen). Samples were incubated with a 1:100 dilution of primary antibodies at 4°C overnight before washing three times over 3 h or overnight in PBTX and blocking again for 1–2 h (this step was omitted for samples treated with anti-mouse 555 only). Following the second block, samples were incubated with secondary antibodies at 1:100 dilution for 8 h or overnight at 4°C before a minimum of four 30 min washes in PBTX. Samples were then mounted in 60% glycerol/PBS. Older samples were cleared before imaging to increase clarity at depths over 100 μm. Samples were dehydrated in a methanol series (25%, 50%, 70%, 100%, 100%, for 3 minutes each) then cleared in a 2:1 solution of Benzyl benzoate: Benzyl alcohol (Sigma). Samples obtained from 12.5 dpc embryos or younger were mounted on single concave microscope slides (Sail). Older samples were mounted in 3.5 cm glass bottom culture dishes (Mattek). The final stage of clearing was performed on the mounting apparatus so the samples were not lost. All samples were imaged on a Zeiss LSM 510 META inverted confocal microscope.

Image capture and processing

For collection of data for modeling, samples were imaged at 0.7 × digital magnification on a 20 × objective. Serial optical sections were taken throughout the depth of each sample with each image representing a 5 μm thick section of the field of view. Typically, two or more fields of view were required to provide complete coverage of the sample. Optical sections were exported as an image series then manually aligned and joined. Custom-built macros generated with the ‘Actions’ feature in Adobe Photoshop were used to repeat the joining and alignment process for subsequent images in the series.

3D modelling

Joined image stacks were imported into the tomography program IMOD http://bio3d.colorado.edu/imod/ (Kremer et al., 1996). Testis cords and other features of interest were outlined in each optical section throughout the image stack then meshed together and rendered to create a three-dimensional representation of the tissue structure in

the sample. Z-depth was adjusted to the thickness of each slice to give an accurate representation of the volume of the sample.

Analysis of gene expression patterns from GUDMAP database

Testis-specific gene expression patterns were retrieved from www.gudmap.org/ in November 2008 by searching for genes where expression is present in testis from Theiler stage (TS) 21, which corresponds to 13.5 dpc. The search results consisted of images which were individually assessed to determine specificity of the expression pattern depicted by comparison to levels of background staining in surrounding tissue. If the expression pattern was deemed to be specific, then the localisation of the gene was annotated with reference to known tissue compartments or apparent expression domains.

Supplementary Material

Refer to Web version on PubMed Central for supplementary material.

Acknowledgments

We thank Andrew Noske, Adam Costin, and Garry Morgan for their help with IMOD, and Terje Svingen for critically reading the manuscript. Confocal microscopy was performed at the ACRF/IMB Dynamic Imaging Centre for Cancer Biology, established with the support of the Australian Cancer Research Foundation. This work was supported by the Australian Research Council, the National Health and Medical Research Council of Australia, and the National Institutes of Health (USA).

Grant information: Grant sponsor: NHMRC Australia; Grant number 334314.

Grant sponsor: National Institutes of Health; Grant number DK070136.

References

Buehr M, Gu S, McLaren A. Mesonephric contribution to testis differentiation in the fetal mouse. Development. 1993a; 117:273–281. [PubMed: 8223251]

Buehr M, McLaren A, Bartley A, Darling S. Proliferation and migration of primordial germ cells in We/We mouse embryos. Dev Dyn. 1993b; 198:182–189. [PubMed: 8136523]

Bullejos M, Koopman P. Spatially dynamic expression of Sry in mouse genital ridges. Dev Dyn. 2001; 221:201–205. [PubMed: 11376487]

Catala M, Teillet MA, De Robertis EM, Le Douarin ML. A spinal cord fate map in the avian embryo: while regressing, Hensen's node lays down the notochord and floor plate thus joining the spinal cord lateral walls. Development. 1996; 122:2599–2610. [PubMed: 8787735]

Combes AN, Wilhelm D, Davidson T, Dejana E, Harley V, Sinclair A, Koopman P. Endothelial cell migration directs testis cord formation. Developmental Biology. 2008

Cool J, Carmona FD, Szucsik JC, Capel B. Peritubular myoid cells are not the migrating population required for testis cord formation in the XY gonad. Sex Dev. 2008; 2:128–133. [PubMed: 18769072]

Coveney D, Cool J, Oliver T, Capel B. Four-dimensional analysis of vascularization during primary development of an organ, the gonad. Proc Natl Acad Sci U S A. 2008; 105:7212–7217. [PubMed: 18480267]

Frojdman K, Paranko J, Kuopio T, Pelliniemi LJ. Structural proteins in sexual differentiation of embryonic gonads. Int J Dev Biol. 1989; 33:99–103. [PubMed: 2485707]

Frojdman K, Paranko J, Virtanen I, Pelliniemi LJ. Intermediate filaments and epithelial differentiation of male rat embryonic gonad. Differentiation. 1992; 50:113–123. [PubMed: 1499878]

Gassei K, Schlatt S. Testicular morphogenesis: comparison of in vivo and in vitro models to study male gonadal development. Ann N Y Acad Sci. 2007; 1120:152–167. [PubMed: 18184913]

Hargrave M, Bowles J, Koopman P. In situ hybridization of whole-mount embryos. Methods Mol Biol. 2006; 326:103–113. [PubMed: 16780196]

Karl J, Capel B. Three-dimensional structure of the developing mouse genital ridge. Philos Trans R Soc Lond B Biol Sci. 1995; 350:235–242. [PubMed: 8570687]

Kim Y, Kobayashi A, Sekido R, DiNapoli L, Brennan J, Chaboissier MC, Poulat F, Behringer RR, Lovell-Badge R, Capel B. Fgf9 and Wnt4 act as antagonistic signals to regulate mammalian sex determination. PLoS Biol. 2006; 4:e187. [PubMed: 16700629]

Kremer JR, Mastronarde DN, McIntosh JR. Computer visualization of three-dimensional image data using IMOD. J Struct Biol. 1996; 116:71–76. [PubMed: 8742726]

Little MH, Brennan J, Georgas K, Davies JA, Davidson DR, Baldock RA, Beverdam A, Bertram JF, Capel B, Chiu HS, Clements D, Cullen-McEwen L, Fleming J, Gilbert T, Herzlinger D, Houghton D, Kaufman MH, Kleymenova E, Koopman PA, Lewis AG, McMahon AP, Mendelsohn CL, Mitchell EK, Rumballe BA, Sweeney DE, Valerius MT, Yamada G, Yang Y, Yu J. A high-resolution anatomical ontology of the developing murine genitourinary tract. Gene Expr Patterns. 2007; 7:680–699. [PubMed: 17452023]

Martineau J, Nordqvist K, Tilmann C, Lovell-Badge R, Capel B. Male-specific cell migration into the developing gonad. Curr Biol. 1997; 7:958–968. [PubMed: 9382843]

McMahon AP, Aronow BJ, Davidson DR, Davies JA, Gaido KW, Grimmond S, Lessard JL, Little MH, Potter SS, Wilder EL, Zhang P. GUDMAP: the genitourinary developmental molecular anatomy project. J Am Soc Nephrol. 2008; 19:667–671. [PubMed: 18287559]

Merchant-Larios H, Moreno-Mendoza N, Buehr M. The role of the mesonephros in cell differentiation and morphogenesis of the mouse fetal testis. Int J Dev Biol. 1993; 37:407–415. [PubMed: 8292535]

Orvis GD, Behringer RR. Cellular mechanisms of Mullerian duct formation in the mouse. Dev Biol. 2007; 306:493–504. [PubMed: 17467685]

Paranko J. Expression of type I and III collagen during morphogenesis of fetal rat testis and ovary. Anat Rec. 1987; 219:91–101. [PubMed: 3688465]

Paranko J, Pelliniemi LJ, Vaheri A, Foidart JM, Lakkala-Paranko T. Morphogenesis and fibronectin in sexual differentiation of rat embryonic gonads. Differentiation. 1983; 23 Suppl:S72–S81. [PubMed: 6444179]

Pelliniemi LJ, Paranko J, Grund SK, Frojdman K, Foidart JM, Lakkala-Paranko T. Extracellular matrix in testicular differentiation. Ann N Y Acad Sci. 1984; 438:405–416. [PubMed: 6598325]

Pohl M, Stuart RO, Sakurai H, Nigam SK. Branching morphogenesis during kidney development. Annual Review of Physiology. 2000; 62:595–620.

Scholer HR, Dressler GR, Balling R, Rohdewohld H, Gruss P. Oct-4: a germline-specific transcription factor mapping to the mouse t-complex. Embo J. 1990; 9:2185–2195. [PubMed: 2357966]

Tilmann C, Capel B. Mesonephric cell migration induces testis cord formation and Sertoli cell differentiation in the mammalian gonad. Development. 1999; 126:2883–2890. [PubMed: 10357932]

Wartenberg H, Kinsky I, Viebahn C, Schmolke C. Fine structural characteristics of testicular cord formation in the developing rabbit gonad. J Electron Microsc Tech. 1991; 19:133–157. [PubMed: 1721087]

Wilhelm D, Martinson F, Bradford S, Wilson MJ, Combes AN, Beverdam A, Bowles J, Mizusaki H, Koopman P. Sertoli cell differentiation is induced both cell-autonomously and through prostaglandin signaling during mammalian sex determination. Dev Biol. 2005; 287:111–124. [PubMed: 16185683]

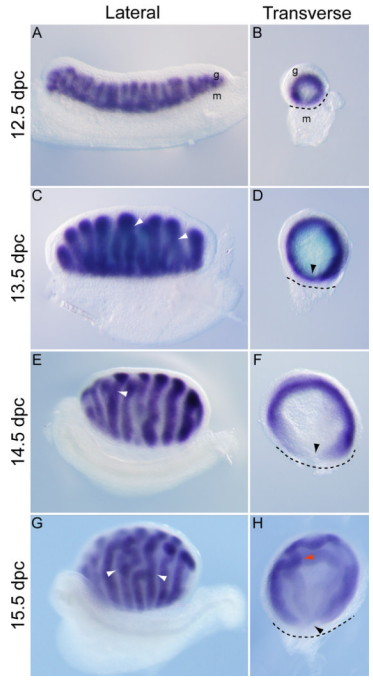

Figure 1.

Testis cord structure visualised by wholemount in situ hybridisation for germ cell marker *Oct-4*. (A–H) Lateral and transverse views of cord structure in 12.5 – 15.5 dpc testes. From 13.5 dpc evidence of cord overlap and branching were observed (white arrowheads) as well as a change in the transverse profile of the testis cords at the border between gonad and mesonephros (black arrowheads, boundary denoted by dashed line). The mesonephros has been removed in D,F,H. From 15.5 dpc some cords buckled under the coelomic epithelium (red arrowhead). g, gonad; m, mesonephros.

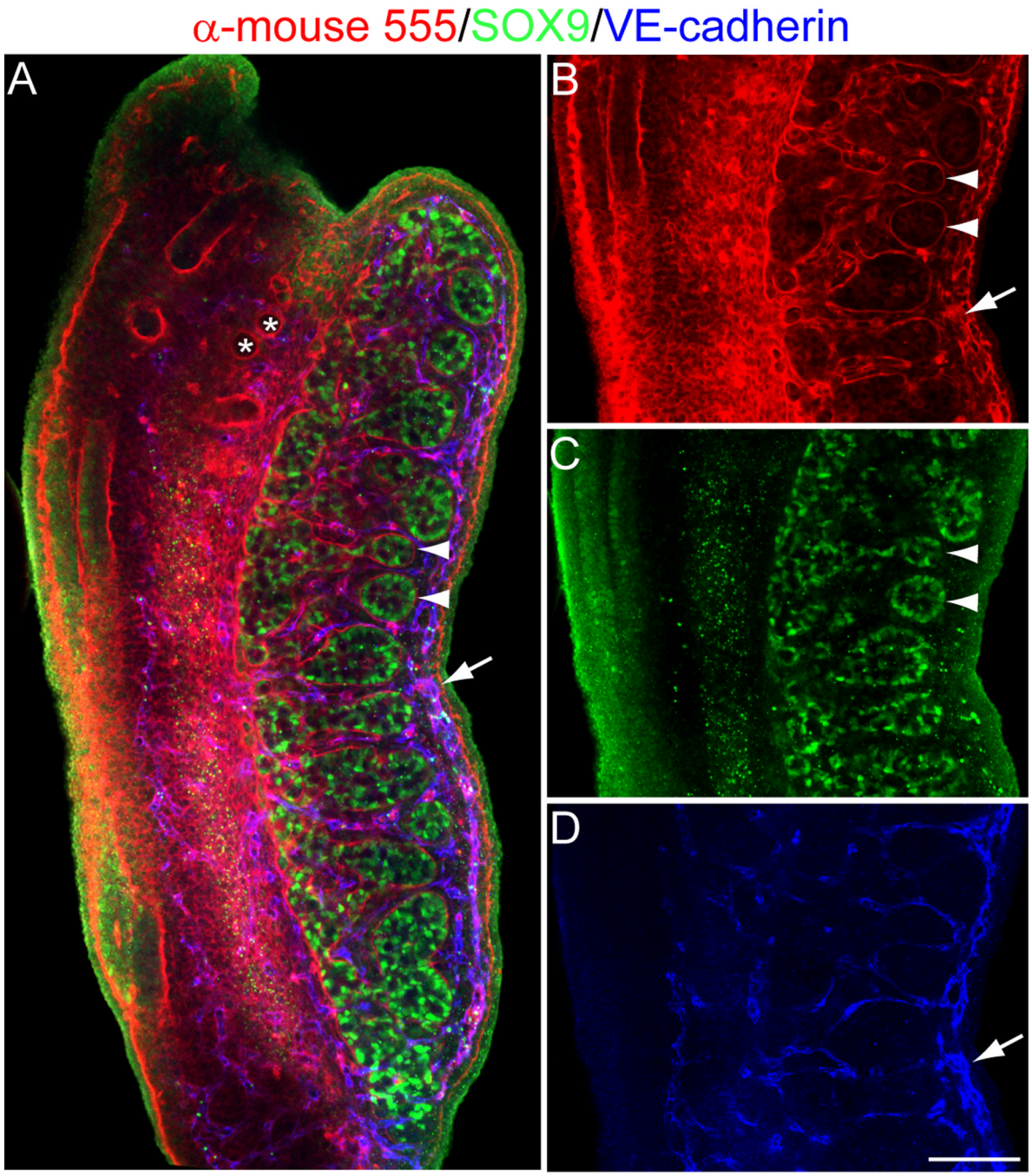

Figure 2.
Validation of 555 antibody. (A) Structures labelled by 555 (red) were compared to Sertoli (green) and vascular (blue) markers to determine that this antibody outlined the basement membrane around the testis cords (arrowheads), the mesonephric tubules (asterisks) as well as marking the vasculature (arrow) and the interstitium. (B–D) Single channel images for the 555, SOX9, and VE-cadherin fluorescence respectively. Scale bar, 100 μm.

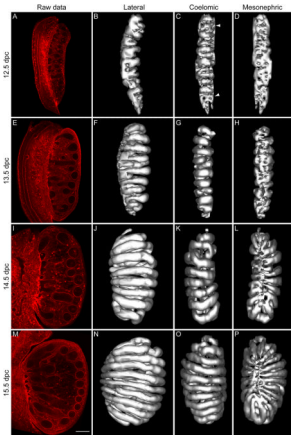

Figure 3.

Testis cord modelling visualised with 555. (A–P) Lateral, coelomic, and mesonephric views of models generated from testis cord outlines from whole mount testis. The left panel in each row is a representative image from the data set used to compile the models. Arrowheads in C indicate areas of irregular, interconnected or perforated, immature cord structures at the gonad poles. Scale bar, 100μm.

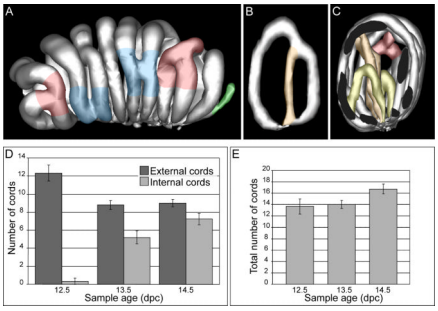

Figure 4.

Testis cord features and numbers. (A) Medial view of the 14.5 dpc model shown in Fig. 3J–L revealing different forms of cord branching. Some cords split at branch points (red) whereas others are fused (blue). A rare blunt-ended cord is indicated (green). (B) A transverse view of a single cord demonstrating an internal branch (orange). (C) Transverse cut-away view (black = cut plane) of a model revealing internal cord structure. Internal cords either branch from external cords (orange) or exist as independent loops (yellow) within the internal space. A three-way branch point is also seen (red). (D) The number of external cords decreases in gonads between 12.5 and 14.5 dpc while the number of internal cords increases. (E) Although the numbers of external and internal cords change as the gonad grows, the total number of cords is relatively stable between 12.5 and 13.5 dpc, increasing slightly at 14.5 dpc. Bars represent the standard error of the mean. For analyses 12.5 *n*=3; 13.5 *n*=5; 14.5 *n*=4.

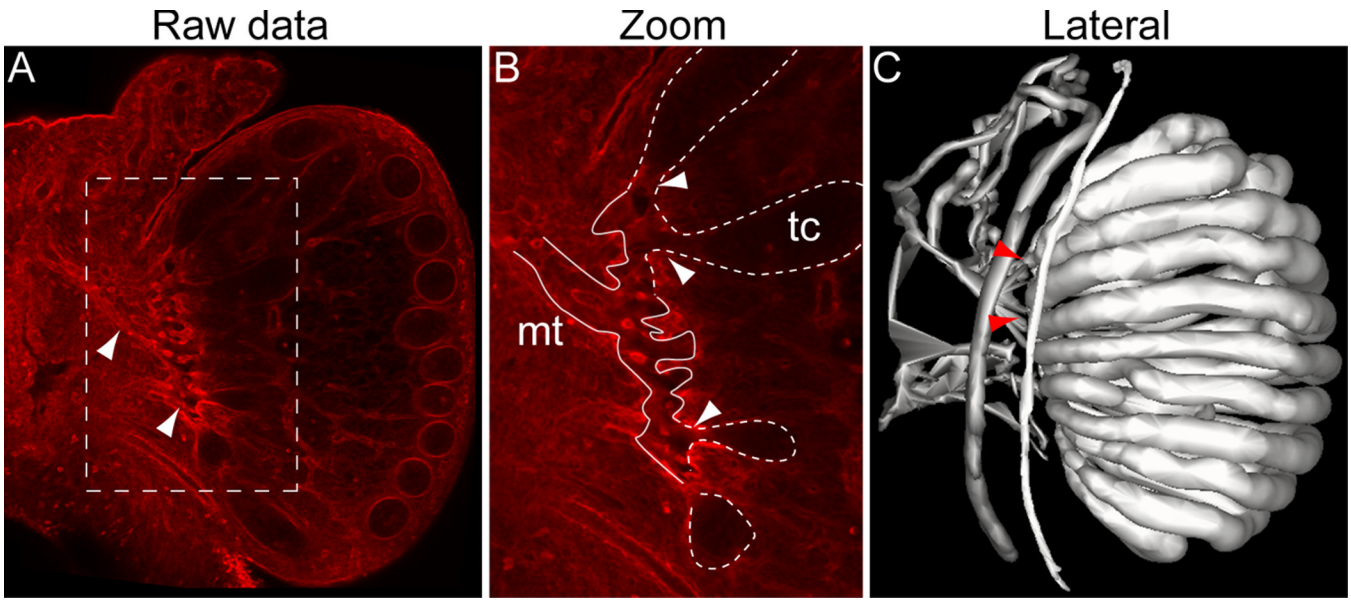

Figure 5.

The plexus at the mesonephric side of the gonad is the precursor of the rete testis. (A) Representative image of a 15.5 dpc testis showing continuity from the testis cords to the mesonephric tubules (arrowheads) through the plexus. (B) Higher magnification of the area boxed in A with connections between testis cords highlighted (arrowheads). Testis cords (tc) are traced with a dashed line, mesonephric tubules (mt) with a solid line. (C) Lateral view of a model showing connectivity between testis cords and the mesonephric tubules. Connections are labelled with red arrowheads.

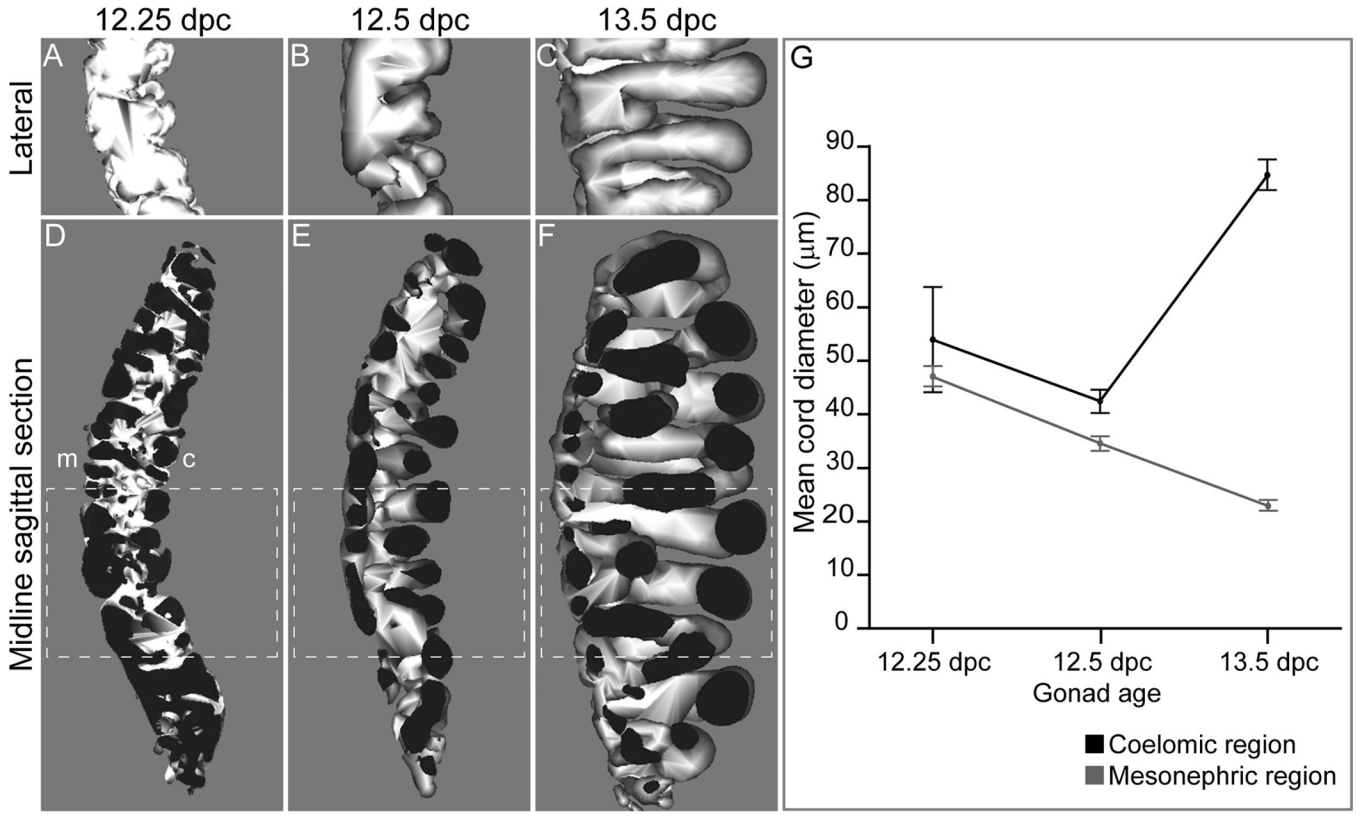

Figure 6.

Testis cord remodelling. (A) Lateral views of models at 12.25 dpc show little evidence of cord partitioning when compared to models at (B) 12.5 dpc or (C) 13.5 dpc. (D–F) Internal views (black = cut plane) of the same samples show extensive segregation of the gonad into irregular cord domains at 12.25 dpc in both mesonephric (m) and coelomic (c) regions, which resolve into more regular structures by 12.5 dpc. By 13.5 dpc, cord structures in the mesonephric region have decreased in diameter, whereas cords under the coelomic surface increased in diameter. The dashed box indicates the region of these models depicted in panels A–C. (G) Changes in mean diameter between cords in mesonephric and coelomic regions. Cord diameters were calculated from ≥ 3 gonads at each age. Bars depict the standard error of the mean.